Eur. Phys. J. Special Topics **229**, 239–251 (2020)

https://doi.org/10.1140/epjst/e2019-900143-8

THE EUROPEAN PHYSICAL JOURNAL SPECIAL TOPICS

Regular Article

Effect of tiny amount of impurity and convective transport on dendrite growth kinetics

Oleg V. Kazak[1,a], Dmitri V. Alexandrov[1], and Peter K. Galenko[1,2]

[1] Ural Federal University, Department of Theoretical and Mathematical Physics, Laboratory of Multi-Scale Mathematical Modeling, 620000 Ekaterinburg, Russia
[2] Friedrich-Schiller-Universität-Jena, Faculty of Physics and Astronomy, Otto Schott Institute of Materials Research, 07743 Jena, Germany

Received 16 July 2019 / Received in final form 7 October 2019
Published online 11 February 2020

Abstract. Using the developed sharp-interface model of solidification we quantitatively estimate influence of tiny amount of impurity and forced convection on kinetics of dendritic growth. As tested systems, we choose Ni and Ni–Zr dendrites which are growing into a stagnant undercooled melt, the melt with incoming forced flow and with/without impurity (that is small amount of Zr diluted in a pure Ni). The model predictions and comparisons allow us to quantitatively estimate predominant influence of impurity (chemical segregation), thermal influence (due to temperature inhomogeneity) and hydrodynamic effects (due to investigated laminar and forced melt flow) on the dendrite growth kinetics.

1 Introduction

Small amounts of impurity and convective flow may drastically influence on the growth kinetics of crystals [1,2]. It has been shown in a number of experimental and computational works. For instance, small amounts of impurities on the level of 0.01 at. % may lead to an enhancement of the growth velocity in the range of small and intermediate undercoolings [3–7] and the convective flow may have an influence pure Ni and Ti as well as on the alloying systems such as Ni–Al, Ni–Cu, Ti–Al, Ni–Zr solidifying under terrestrial conditions, in microgravity and under the influence of external fields [8–20].

On the basis of these investigations, it was suggested that the solute effect shows a different temperature characteristics than the transport effect by fluid flow, which makes it possible to discriminate between both these effects by investigating the dendritic growth velocity as a function of undercooling [4–7,10]. In the present work we test this idea using the sharp interface modeling of dendritic solidification (for the model development, see Refs. [16,17], literature references there and supplementary materials). To see the predominant influence of flow and/or impurity we compare results of modeling for solidification of Ni and Ni–Zr alloys in a wide range of undercooling.

[a] e-mail: olegkazak@yandex.ru

2 Governing equations

The growth of a parabolic needle-like dendrite in a binary undercooled liquid in local non-equilibrium conditions can be described by the stable dendrite growth model provided in [16]. We consider the atomic diffusion in the solid phase to be negligible. The concentration field in the liquid is governed by the following mass transport equation

$$\tau_D \frac{\partial^2 C_l}{\partial t^2} + \frac{\partial C_l}{\partial t} + (\mathbf{w} \cdot \nabla) C_l = D_C \nabla^2 C_l, \tag{1}$$

where C_l is the solute concentration in the liquid, $\mathbf{w}$ is the flow velocity, D_C is the diffusion coefficient of the solute, t is the time and τ_D is the relaxation time of the diffusion flux to its steady state.

The mass transport can be described by the hyperbolic equation (1) which includes the finite value of the diffusion speed $V_D = (D_C/\tau_D)^{1/2}$, the evolution of the temperature field is described by a parabolic equation which assumes an infinite speed for the heat propagation.

Designating T_l and T_s as temperatures in the liquid and solid phases, one can write

$$\frac{\partial T_l}{\partial t} + (\mathbf{w} \cdot \nabla) C_l = D_T \nabla^2 T_l, \quad \frac{\partial T_s}{\partial t} = D_T \nabla^2 T_s, \tag{2}$$

where D_T stands for the thermal diffusivity.

At the dendritic interface, conservation of mass and energy yields boundary conditions of the form

$$\tau_D \frac{\partial}{\partial t} \left[(C_l - C_s) \mathbf{v} \cdot \mathbf{n} \right] + (C_l - C_s) \mathbf{v} \cdot \mathbf{n} + D_C \nabla C_l \cdot \mathbf{n} = 0, \tag{3}$$

$$T_Q \mathbf{v} \cdot \mathbf{n} = D_T \left(\nabla T_s - \nabla T_l \right) \cdot \mathbf{n}, \tag{4}$$

where $\mathbf{n}$ is the unit vector normal to the dendrite interface, $\mathbf{v}$ is the interface velocity, $C_s = k_v C_l$ is the concentration in the solid phase at the dendritic interface, k_v is the velocity dependent solute distribution coefficient, $T_Q = Q/c_p$, Q is the latent heat released per unit volume of solidified matter and c_p is the heat capacity.

The temperature at the dendrite interface $T_i = T_{l;i} = T_{s;i}$ is connected to the crystallization temperature T_0 of the pure liquid, the local curvature $2/R$ of the front, the liquid concentration C_l, and the intensity of atomic flux providing the normal growth velocity $(\mathbf{v} \cdot \mathbf{n}) = v_n$ by

$$T_i = T_0 + m_v C_l - Q c_p^{-1} 2 R^{-1} d(\theta) - \tilde{\beta}(\theta) v_n. \tag{5}$$

Here θ is the angle between the normal to the dendrite interface and its preferred growth direction (e.g., $\langle 001 \rangle$ directions for cubic crystals), $\tilde{\beta}$ is the anisotropic coefficient of growth, $d(\theta)$ is the anisotropic capillary length, and m_v is the velocity-dependent liquidus line slope in the kinetic phase diagram of a binary system.

Anisotropic properties of the interface, such as surface energy, depend on the spherical angles which define the orientation of the normal to the dendrite interface to its growth direction. Considering a case of axisymmetric needle-like crystal one can apply averaging over one spherical angle and essentially simplify analytical form of the anisotropic properties of the crystal-liquid interface [21]. As a result of such averaging for the cubic crystal symmetry, the capillary length $d(\theta)$ and kinetic coefficient $\widetilde{\beta}(\theta)$ are represented as

$$d(\theta) = d_0 \left\{ 1 - \alpha_d \cos \left[4 \left(\theta - \theta_d \right) \right] \right\}, \tag{6}$$

$$\tilde{\beta}(\theta) = \beta_0 Q c_p^{-1} \left\{ 1 - \alpha_\beta \cos \left[4 \left(\theta - \theta_\beta \right) \right] \right\}, \tag{7}$$

where d_0 and β_0 are the capillary and kinetic constants, $\alpha_d \ll 1$ and $\alpha_\beta \ll 1$ are the anisotropy parameters whereas θ_d and θ_β represent the angles between the direction of growth and the preferred growth directions, which correspond to the minima of $d(\theta)$ and $\beta(\theta)$.

Far from the dendritic surface the solute concentration, the temperature and the flow velocity in the liquid are fixed, i.e.

$$C_l = C_\infty, \quad T_l = T_\infty, \quad |\mathbf{w}| = U, \tag{8}$$

where U being the characteristic flow velocity far from the dendrite. A family of exact solutions of the hydrodynamic problem can be found in two cases when the fluid flow is potential or of Oseen type. Here, the more realistic case of viscous flow described by the so-called Oseen and mass conservation equations is considered:

$$U\frac{\partial \mathbf{w}}{\partial z} = -\frac{1}{\rho_\ell}\nabla p + \nu\nabla^2\mathbf{w}, \quad \nabla\cdot\mathbf{w} = 0, \tag{9}$$

where z is the direction of dendritic growth, ρ_ℓ is the liquid density and ν is the kinematic viscosity. Equation (9) should be solved with no-slip boundary conditions for the fluid velocity.

The system of equations (1)–(9) couples the concentration and the thermal problem and describes the growth of a parabolic dendrite under local non-equilibrium conditions. It extends the previous problem considered by Ben Amar and Péclet [22] for anisotropic dendrite growth under local equilibrium conditions, generalizes the study of [11] for sufficiently large growth rates in the local equilibrium limit, and, finally, advances the isotropic description [23,24] of the local non-equilibrium dendrite growth.

3 Selection criterion

Consider the steady state tip of a needle-like dendrite with radius R propagating with constant velocity $v_n = V$ and having the tip concentration the liquid phase as $C_l = C_i$. The selection criterion for the steady state dendritic growth can be found by the combination of previously obtained solutions, which describe the anisotropic dendrite growing in the presence of convective flow [13] and the local non-equilibrium dendritic growth in rapid solidification processes without convection [25].

In searching and sewing the criteria, we have assumed that the final selection criterion σ^* must have the scaling $\sigma^* \propto \beta^n$ with the same exponent n and the same general form [21] if the anisotropy for three dimensional or two dimensional spaces are taken into account [25]. An existence of the same scalings in these cases has been shown in [26,27] in which a difference consists only in a constant of proportionality for the scaling $\sigma^* \propto \beta^n$. Therefore, in the present selection criterion σ^* we shall use the case of simplest form of anisotropy given by (6) and (7) under the assumption that the final scaling might be applied to the three dimensional case of dendrite growth. As a result, the selection criterion for the thermo-solutal dendritic growth in non-isothermal binary mixture with convection can be expressed as

$$\sigma^* = \frac{2d_0D_T}{R^2V} \equiv \frac{d_0V}{2D_TP_T^2} = \frac{\sigma_0\alpha_d^{7/4}}{1+b\left(\bar{\alpha}/\alpha_d^{3/4}\right)^{11/14}}\left\{\frac{1}{\left[1+a_1\sqrt{\alpha_d}P_T\Lambda_T\right]^2}\right.$$
$$\left. + \frac{2(1-k_v)m_vC_iD_{TC}}{T_Q\left[1+a_2\sqrt{\alpha_d}P_{CD}^*\Lambda_C\right]^2}\left[1+\chi\left(1-\frac{1}{\sqrt{1-W^2}}\right)\right]^2\right\}, \tag{10}$$

where all functions and parameters are given in Table 1 and in [13], in particular, the thermal Péclet number P_T, chemical Péclet number P_{CD}, flow Péclet number P_f, and Reynolds number Re are defined by

$$P_T = \frac{RV}{2D_T}, \quad P^*_{CD} = \frac{P_{CD}}{\sqrt{1-W^2}}, \quad P_{CD} = \frac{RV}{2D_C},$$
$$P_f = \frac{RU}{2D_T}, \quad \mathrm{Re} = \frac{RU}{\nu}, \tag{11}$$

with the velocity dependent functions and parameters

$$a(\mathrm{Re}) = \frac{\exp(-\mathrm{Re}/2)}{\mathrm{E}_1(\mathrm{Re}/2)}, \quad W = \frac{V}{V_D}, \quad \bar{\alpha} = (1+2D_{TC})\frac{a(\mathrm{Re})Ud_0}{4RVP},$$
$$P = 1 + \frac{2m_vC_i(1-k_v)D_{TC}}{T_Q}, \quad P_0 = P_f + P_T, \tag{12}$$

and the concentration dependent functions

$$C_i = \frac{C_\infty}{1-(1-k_v)P_{CD}I_C\exp\left(P_0D_{TC}\right)},$$
$$I_C = \int_1^\infty \exp\left[2P_fD_{TC}\int_1^{\eta'}\frac{g(\eta'')}{\sqrt{\eta''}}d\eta'' - P_0D_{TC}\eta'\right]\frac{d\eta'}{\eta'},$$
$$g(\eta) = \frac{\sqrt{\eta}\mathrm{E}_1(\mathrm{Re}\ \eta/2)}{2\mathrm{E}_1(\mathrm{Re}/2)} + \frac{\exp(-\mathrm{Re}/2)-\exp(-\mathrm{Re}\ \eta/2)}{\sqrt{\eta}\mathrm{Re}\mathrm{E}_1(\mathrm{Re}/2)},$$
$$\mathrm{E}_1(q) = \int_q^\infty \frac{\exp(-u)}{u}du, \tag{13}$$

and parameters

$$D_{TC} = \frac{D_T}{D_C}, \ a_1 = \frac{a_2}{\sqrt{2}}, \ a_2 = \left(\frac{16\sigma_0}{7}\right)^{1/2}\left(\frac{3}{56}\right)^{3/8},$$
$$\chi^2 = \frac{4}{7}\left(\frac{3}{56}\right)^{3/4}\alpha_d^{-3/4}, \ \Lambda_T = 1+\frac{\delta_0D_T\beta_0}{d_0}, \ \Lambda_C = 1+\frac{\delta_0D_C\beta_0}{d_{0CD}},$$
$$\delta_0 = 20\sqrt{\frac{7}{24}}\left(\frac{56}{3}\right)^{3/8}, \ d_{0CD} = \frac{T_Qd_0}{2m_eC_i(1-k_e)}. \tag{14}$$

Note that the anisotropy of growth kinetics α_β does not enter in the selection criterion (10). This is due to the fact that terms with α_β contain terms of higher order (and therefore with smaller values) than the terms taken into account in the linear instability analysis carried out in [13].

Equation (10) contains previously known criteria of the following limiting cases. First, in the absence of convection ($U = 0$, $\bar{\alpha} = 0$) and solute concentration ($C_i = 0$) this criterion transforms to the well-known expression $\sigma^* = \sigma_0\alpha_d^{7/4}$ derived for the first time by Langer, Hong, Péclet and Bensimon [28,29] in the limit of small Péclet number ($P_T \to 0$). Second, at small growth velocities ($P_T \ll 1$, $P_{CD} \ll 1$ and $W \ll 1$) and with $U = 0$, criterion (10) reduces to the criterion derived by Ben Amar and Péclet [22]. Third, in the case of a pure material ($C_i = 0$) and small

growth rates ($P_T \ll 1$ and $W \ll 1$) equation (10) coincides with the selection law derived by Bouissou and Péclet [30]. Fourth, in the limit of small Péclet numbers ($P_T \to 0$, $P_{CD} \to 0$) within the framework of the parabolic mass transfer mechanism ($W = 0$), the criterion (10) corresponds to the previously derived criterion in [12]. Fifth, in the case of stagnant fluid ($U = 0$) and local-equilibrium solidification with arbitrary Péclet numbers ($W = 0$) in the absence of growth kinetics ($\beta_0 = 0$), the aforementioned criterion tends to the interpolation expression obtained by Müller-Krumbhaar et al. [31]. Sixth, at the same assumptions, this criterion transforms to the criterion derived in [11] for the thermo-solutal problem with arbitrary Péclet numbers. Seventh, in the case of a single-component melt ($C_i = 0$) in the limit of small Péclet numbers ($P_T \ll 1$ and $P_{CD} \ll 1$) without convection ($U = 0$) and when $W = 0$ the criterion (10) leads to the selection law found by Brener [32]. Thus, the selection criterion (10) generalizes earlier known criteria on both thermal and diffusion limited dendritic growth.

4 Sharp interface model

The criterion (10) selects the unique combination of the dendrite tip radius R and dendrite tip velocity V from the family of needle-like shapes under convective flow. The present section shows how these selected values of R and V are related to the experimentally controlled parameter of the process, the total undercooling ΔT.

The framework of a model for the dendritic tip growth has been established in the works [33,34], which was extended to the case of rapid solidification in [35–38] and finally to the local non-equilibrium case in [23,24]. The basic idea of these works consists of the combination of a selection criterion with the balance of undercooling contributions at the dendritic tip.

The total undercooling $\Delta T = T_0 - m_e C_\infty - T_\infty$, represents the undercooling balance at the dendrite tip as

$$\Delta T = \Delta T_T + \Delta T_C + \Delta T_N + \Delta T_R + \Delta T_K, \tag{15}$$

where C_∞ and T_∞ are the initial (i.e. far-field) composition and temperature in the alloy, respectively, ΔT_T is the thermal undercooling, ΔT_C is the constitutional undercooling, $\Delta T_N = (m_e - m_v)C_\infty$ is the undercooling arising due to the shift of the equilibrium liquidus line from its equilibrium position in the kinetic phase diagram of steady-state solidification, $\Delta T_R = 2d_0 T_Q / R$ is the curvature undercooling due to the Gibbs-Thomson effect and $\Delta T_K = V/\mu_k$ is the kinetic undercooling corresponding to the kinetic growth coefficient μ_k. Equation (15) connects the temperature T_i and concentration C_i at the dendrite tip [see Eq. (5)] with the temperature T_∞ and concentration C_∞ in the bulk of the undercooled melt, showing a full consistency of equations (5) and (15).

The convection effects will change the heat and mass transport around the growing dendrite from the standard Ivantsov solution. The thermal undercooling ΔT_T is defined by the modified Ivantsov function $\mathrm{Iv}^*(P_T, P_f)$ as

$$\Delta T_T = T_Q \mathrm{Iv}^*(P_T, P_f). \tag{16}$$

Here the modified Ivantsov function for the conductive and convective heat transport is described by

$$\mathrm{Iv}^*(P_T, P_f) = P_T \exp(P_T + P_f) I_T(P_T, P_f), \tag{17}$$

with the integral

$$I_T(P_T, P_f) = \int_1^\infty \exp\left[2P_f \int_1^{\eta'} \frac{g(\eta'')}{\sqrt{\eta''}} d\eta'' - P_0 \eta'\right] \frac{d\eta'}{\eta'},$$

which is completely analogous to the integral in equation (13) (see [12]). The constitutional undercooling ΔT_C is expressed as

$$\Delta T_C = k_v \Delta_v \frac{\mathrm{Iv}^*(P_{CD}, P_f)}{1-(1-k_v)\mathrm{Iv}^*(P_{CD}, P_f)}, \quad V < V_D,$$
$$\Delta T_C = 0, \qquad V \geq V_D, \tag{18}$$

where the modified Ivantsov function for the conductive and convective mass transport follows from the concentration at the dendritic tip in equation (13) as

$$\mathrm{Iv}^*(P_{CD}, P_f) = P_{CD} \exp(P_{CD} + P_f D_{TC}) I_C(P_{CD}, P_f). \tag{19}$$

The velocity dependent non-equilibrium interval Δ_v of solidification in equation (18) is given by

$$\Delta_v = m_v C_\infty (1-k_v)/k_v, \quad V < V_D,$$
$$\Delta_v = 0, \qquad V \geq V_D. \tag{20}$$

Note that if the dendrite tip velocity V is equal to or greater than the solute diffusion speed V_D, the constitutional undercooling ΔT_C is equal to zero, corresponding to the transition to the diffusionless regime of solidification. Obviously, with zero convective velocity ($U = 0$), solutions (16) and (19) revert to the standard Ivantsov functions $\mathrm{Iv}(P_T)$ and $\mathrm{Iv}(P_{CD})$, respectively.

The velocity dependent liquidus slope is described by [39]:

$$m_v = \frac{m_e}{1-k_e}\left\{1 - k_v + \ln\left(\frac{k_v}{k_e}\right) + (1-k_v)^2 \frac{V}{V_D}\right\}, \qquad V < V_D,$$
$$m_v = \frac{m_e \ln k_e}{k_e - 1} \equiv const, \quad V \geq V_D. \tag{21}$$

The velocity-dependent partition coefficient $k_v = C_s/C_i$ is given by [40]:

$$k_v = \frac{(1 - V^2/V_D^2)k_e + V/V_{DI}}{(1 - V^2/V_D^2)[1-(1-k_e)C_i] + V/V_{DI}}, \quad V < V_D,$$
$$k_v = 1, \qquad V \geq V_D. \tag{22}$$

In comparison to previous local equilibrium models, two additional kinetic parameters, V_{DI} and V_D, enter the non-equilibrium partitioning function k_v defined by equation (22) and consequently propagate to the functions ΔT_C, Δ_v, and m_v related to the solute diffusion in the balance of undercoolings (15). A detailed description of values for V_{DI} and V_D is given in [41]. Within the local equilibrium limit in bulk liquid, $V_D \to \infty$, equations (15)–(22) transform into the corresponding equations of the models [36,38] which relax the local equilibrium at the interface by atomic kinetics and interfacial diffusion. In contrast, the present description adopts a finite diffusion velocity in the bulk of undercooled liquid as a further contribution to local non-equilibrium.

The condition in equation (18) for the absence of constitutional undercooling at $V \geq V_D$ results from the analytical solution of the model of solute diffusion, applicable to rapid solidification [23,24]. In such a case, the liquidus and solidus lines merge into one line in the kinetic phase diagram of the alloy and the non-equilibrium interval of solidification becomes exactly zero [see Eq. (20)]. Therefore, the velocity $V = V_D$ is considered as that finite velocity at which complete solute trapping $k_v = 1$ occurs, (22), and beyond which solidification proceeds with the initial (nominal) composition C_∞. At this velocity the transition from solutal to thermal dendrites is completed with the onset of diffusionless solidification and with the beginning of purely thermal growth of dendrites.

Table 1. Material parameters for Ni and NiZr used in calculations as is given in [7,43].

Material parameter	Dimension	Pure Ni	Ni-0.01 at.%Zr	Ni-0.1 at.%Zr	Ni-0.5 at.%Zr	Ni-1 at.%Zr
Nominal concentration, C_∞	at.%	0	0.01	0.1	0.5	1
Melting temperature, T_m	K	1728	1728	1728	1728	1728
Thermal diffusivity, D_T	m^2/s	1.2×10^{-5}	1.2×10^{-5}	1.2×10^{-5}	1.2×10^{-5}	4.2×10^{-5}
Diffusion coefficient, D_C	m^2/s	–	2.8×10^{-9}	2.5×10^{-9}	2.5×10^{-9}	2.5×10^{-9}
Equilibrium partition coefficient, k_e		–	0.02	0.02	0.03	0.04
Liquidus slope, m_e	K/at.%	–	−9	−9	−10	−11
Capillary constant, d_0	m	7.89×10^{-10}	7.89×10^{-10}	7.89×10^{-10}	7.89×10^{-10}	2.02×10^{-10}
Kinetic growth coefficient, μ_k	$m/s/K$	0.59	0.59	0.59	0.42	0.22
Strength of the surface energy anisotropy, α_d	0.66	0.66	0.66	0.675	0.75	
Bulk diffusion speed, V_D	m/s	–	23.5	23.5	21.5	21
Interface diffusion speed, V_{DI}	m/s	–	22.5	22.5	20	20.5
Latent heat of crystallization, Q	J/mol	17150	17150	17150	16700	16230
Heat capacity, c_p	J/mol/K	41	41	41	41	41
Density, ρ_ℓ	kg/m^3	8.1×10^3	8.1×10^3	8.1×10^3	8.1×10^3	8.1×10^3
Dynamic viscosity, η	$Pa \cdot s$	4.3×10^{-3}	4.3×10^{-3}	4.3×10^{-3}	4.3×10^{-3}	4.3×10^{-3}

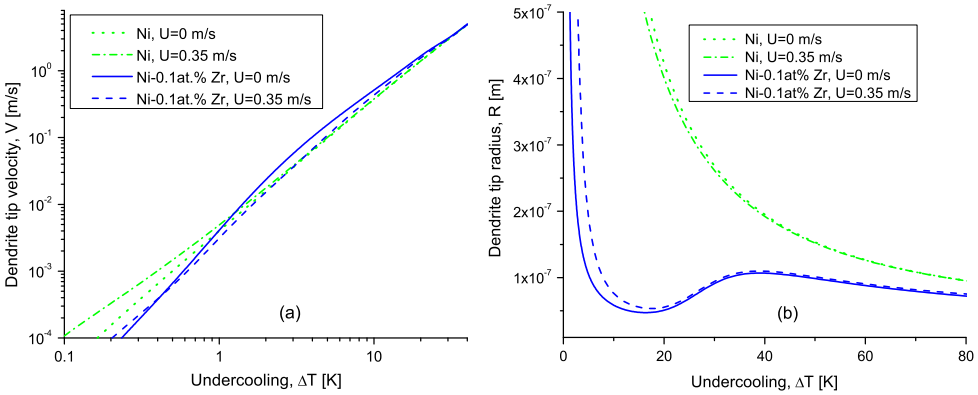

Fig. 1. (a) Dendrite tip velocity V as a function of undercooling ΔT in pure Ni and Ni-0.1 at.%Zr. Curves show the different influence of convective flow and alloy concentration on the dendrite tip velocity V when the flow velocity changes from $U = 0\,(\mathrm{m/s})$ to $U = 0.35\,(\mathrm{m/s})$. (b) Dendrite tip radius R as a function of undercooling ΔT for pure Ni and Ni-0.1 at.%Zr. Curves show the different influence of convective flow and alloy concentration on dendrite tip radius when the flow velocity changes from $U = 0\,(\mathrm{m/s})$ to $U = 0.35\,(\mathrm{m/s})$.

5 Results and discussion

To evaluate the effect of convective flow on the dendrite growth from pure and binary melts we have chosen the Ni melt and the melt on Ni with small amounts of Zr. Material parameters of Ni and Ni–Zr are summarized in Table 1.

Figure 1 shows the complicated behavior of dendrite tip velocity V in a wide range of undercooling $\Delta T = 0{-}100\,\mathrm{K}$ for a stagnant melt ($U = 0\,\mathrm{m/s}$) and with incoming forced flow ($U = 0.35\,\mathrm{m/s}$). The chosen velocity of incoming flow is typical for ground based experiments in electromagnetically levitating liquid samples [2,7,10,14,15,19,42] at which one can expect an essential influence of flow on the crystal growth due to their comparable velocities [16]. Such a complicated behavior is seen in multiple crossing of solid and dashed lines $V - \Delta T$ due to the predominant effects of convection or tiny amounts of impurity at different undercooling ranges. To interpret the peculiarities of this behavior Figures 2–5 give the detailed pictures of calculated dependencies.

Figures 2a and 2b show that the addition of a small amount of impurity leads to increasing the growth velocity of the alloying dendrite in comparison with a pure

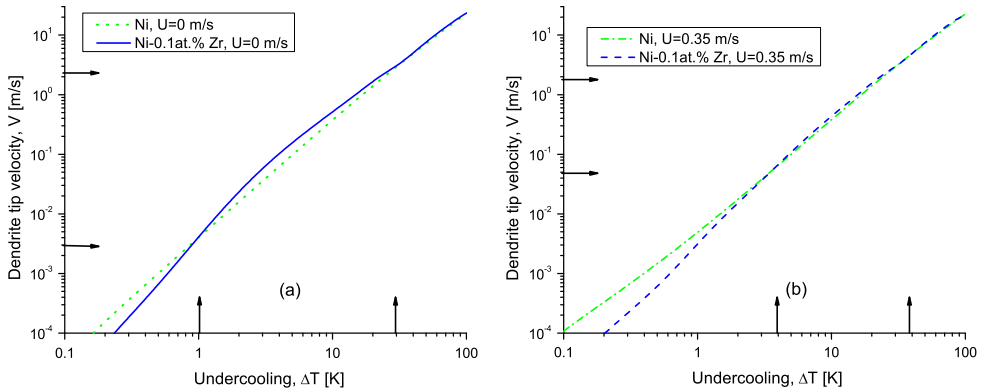

Fig. 2. Intersection of a dendrite tip velocity V curves at given undercoolings ΔT indicated by arrows in pure Ni and Ni-0.1 at.%Zr with flow velocity (a) $U = 0\,(\mathrm{m/s})$ and (b) $U = 0.35\,(\mathrm{m/s})$.

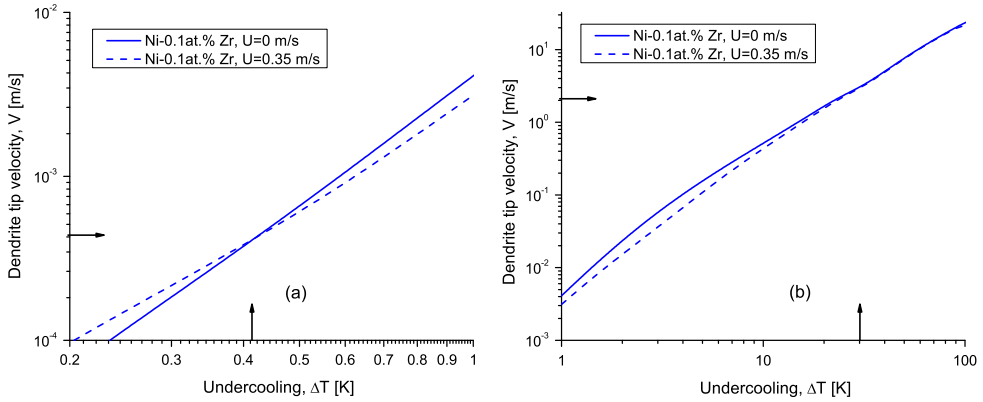

Fig. 3. Intersection of a dendrite tip velocity V curves at given undercoolings ΔT indicated by arrows in pure Ni and Ni-0.1 at.%Zr with flow velocity (a) $U = 0\,(\mathrm{m/s})$ and (b) $U = 0.35\,(\mathrm{m/s})$.

dendrite. It occurs due to the appearance of additional concentrational undercooling appearing due to the presence of small amount of impurity as an additonal driving force. In addition to this, Figures 3a and 3b demonstrate that the convection, which plays a key role at small undercooling (up to $\Delta T \approx 1\,\mathrm{K}$), degenerates at large undercoolings due to much high velocity of dendrite growth.

A very interesting effect can be observed in the range of undercoolings from $\Delta T = 1$ to $\Delta T = 100\,\mathrm{K}$. This effect occurs due to the rejection of solute in a bulk liquid by the growing dendritic surface. An accumulation of solute leads to the concentrational gradients and the appearance of concentrational undercooling. As the result, the velocity of alloying dendrite becomes larger than the growth rate of pure dendrite. With the largest undercoolings all curves merge. This shows the predominant influence of kinetics and nonequilibrium growth effects (solute trapping) over the influence of convective flow.

As is shown in Figure 3a, the convection dominates at small undercooling up to $\Delta T \approx 0.45\,\mathrm{K}$. Then the influence of impurity becomes predominant in comparison with the effect of flow on the alloying dendrite up to $\Delta T \approx 35\,\mathrm{K}$, see Figure 3b. Such an influence has been confirmed in experiments carried out on the ground and under

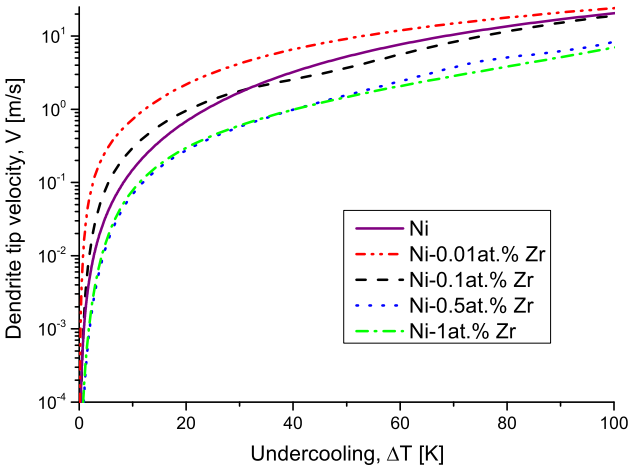

Fig. 4. Effect of dendrite growth velocity enhancement in diluted alloys. It is shown that the tips of very diluted alloying dendrites, Ni-0.01 at.%Zr and Ni-0.1 at.%Zr are growing faster in specific regions of undercooling than the tip of Ni dendrite and also faster than simply diluted alloyed dendrites Ni-0.5 at.%Zr, Ni-1 at.%Zr. The computation has been made for the flow velocity $U = 0\,(\mathrm{m/s})$.

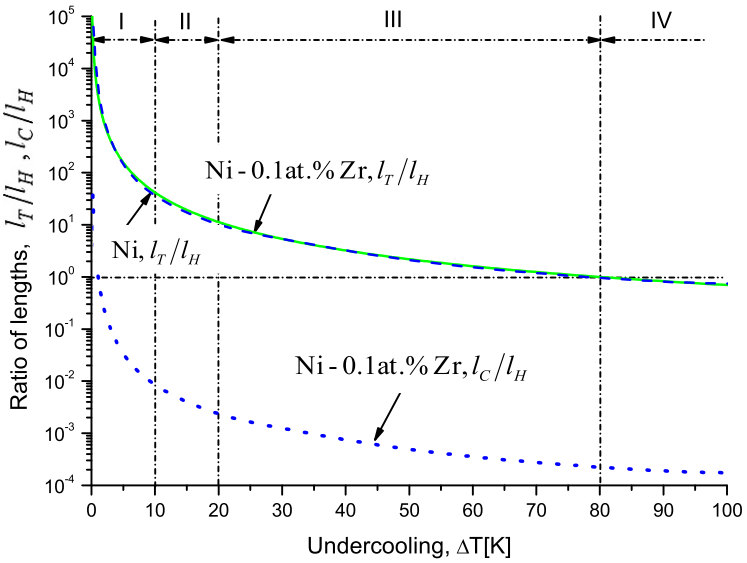

Fig. 5. The thermal length scale ℓ_T and solutal length scale, ℓ_C, in comparison with the hydrodynamic length scale ℓ_H for the growth of Ni and Ni–Zr dendrites, as calculated from equations (23)–(26). Range I: influence of the solutal length scale in concurrence with the effect of fluid flow. Range II: the increase in the thermal length influence. Range III: the predominant influence of the thermal and hydrodynamics transport. Range IV: dendrite growth kinetics do not sensitive to the hydrodynamic motion due to high growth velocity.

reduced gravity [10] as well as in the phase-field modeling [6]. Hence the predominant role of the flow effect appearing in rapid solidification is visible for Ni–Zr alloys at the dendrite growth velocities becomes greater than 1 m/s.

Usually, thicker dendrites grow faster due to existing of the concentrational gradient with the appearing of the concentrational undercooling. However, in some spe-

cific cases thicker dendrites can grow faster due the flow effect of the incoming forced stream. This effect is illustrated in Figure 3 for the Ni–Zr dendrites at undercoolings greater than 20 K (in order of magnitude), where the tip radius R begins to grow with increasing the melt undercooling (the tip velocity V is always an increasing function of ΔT as is demonstrated in Figs. 1–3). Additional increasing of the dendrite tip radius exists due to the presence of a forced flow (compare the dash-dotted and double dash-dotted lines in Fig. 4).

To demonstrate another important effect that the dendrite tip velocity increases as a tiny addition of impurity is added to the pure melt, we illustrate in Figure 4 the growth of Ni–Zr dendrites with tiny inclusions of zirconium in the main solidifying component – nickel. For instance, considering the growth of Ni-0.1at.% Zr dendrite we see that its growth rate exceeds the growth rates of the pure nickel dendrite and of the Ni-0.01at% Zr dendrite in the undercooling range $0 < \Delta T < 35$ K. This confirms a quicker growth of the narrow chemical dendrites with small impurity additions in comparison with thicker thermal dendrites. This effect can be explained by the fact that the tiny amounts of impurity create the additional crystallization sites ahead of the dendritic tip, which in turn adhere to its surface accelerate the growth of dendritic tips.

To quantify the combined influence of the forced flow and the impurity on the process of dendritic solidification, we apply the method of characteristic length scales [16]. For the present analysis these are defined by the thermal length scale l_T, the solutal length scale l_C, and the hydrodynamic length scale l_H as

$$\ell_T = \frac{2D_T}{V},\ \ell_C = \frac{2D_C}{V},\ \ell_H = \frac{\nu}{U}, \tag{23}$$

where ν is the kinematic viscosity. D_T and D_C are already defined earlier and should not be introduced again. Quantitative estimations can be made by a consideration of ratios between length scales (22), which can be calculated for the Ni and Ni–Zr melts using their material parameters listed in Table 1 as

$$\text{Ni}: \text{ and Ni}-\text{Zr}: \quad \frac{\ell_T}{\ell_H} = 15.8234\frac{1}{V}, \tag{24}$$

concentration/hydrodynamics ratio becomes negligible

$$\text{Ni}-\text{Zr}: \quad \frac{\ell_C}{\ell_H} = 2\times 10^{-3}\frac{1}{V}, \tag{25}$$

$$\text{Ni}-\text{Zr}: \quad \frac{\ell_T}{\ell_C} = 4.2857\times 10^{3}. \tag{26}$$

Figure 5 demonstrates these relative ratios as the functions of undercooling in the range $10 < \Delta T < 100$ K at a fixed value of the forced convection, $U = 0.35$ m/s (10^0 corresponds to the scales of equal lengths). For values close to unity, the effect of convection on the kinetics of dendritic growth is greatest.

From the physical point of view, the thermal, solutal, and hydrodynamic processes are capable to interact if their characteristic length scales are of the same order. In the range of sufficiently small undercooling, $1 < \Delta T(K) < 10$ (range I in Fig. 5), the thermal length ℓ_T is large enough ($\ell_T/\ell_H \sim 10^2-10^3$) while the solutal length is smaller, $\ell_C/\ell_H \sim 1-10$. Therefore, the influence of convection is decisive in the range $10 < \Delta T < 20$ K. At the undercooling $10 < \Delta T(K) < 20$ (range II in Fig. 5), there is a transitive regime of growth in which influence of solute falls down but the influence of the thermal transport begins to be essential together with the convective transport. With the further increase in undercooling, $20 < \Delta T(K) < 80$ (range III in

Fig. 5), concentration / hydrodynamics ratio becomes negligible $\ell_C/\ell_H \ll 2 \times 10^{-3}$ but the role of thermal and hydrodynamic transport becomes predominant: $\ell_T/\ell_H \sim 10^0 - 10^1$. Due to the high dendrite velocity ($V > 10\,\mathrm{m/s}$) in comparison with the flow velocity ($U = 0.35\,\mathrm{m/s}$) the convection does not influence on the growth kinetics in the range $\Delta T(K) > 80$. These changes in length scales govern the dendrite growth and predominant influence of solutal, thermal and hydrodynamic transport shown in Figures 1–4.

About the interplay between thermal and solutal length scales, one should mention the following. From Figure 5 it is clearly seen that at the smallest undercooling ($\Delta T < 5\,\mathrm{K}$) the solutal length is close to unity and the thermal length is much higher than unity (in comparison with the hydrodynamic length scale). Figure 5 also shows that with the increase in undercooling up to $\Delta T = 30\,\mathrm{K}$, the solutal length essentially decreases and the thermal length has a tendency coming to unity. Therefore, one can expect to have an interplay between solutal and thermal contributions (namely at $\Delta T < 30\,\mathrm{K}$) that is clearly shown in Figure 2.

In the present section, the length scale analysis has been used to estimate influence of the predominant effect (thermal, solutal or hydrodynamic influence) on the dendrite growth in a wide range of undercooling. To provide data on microstructure and secondary processes (such as coarsening, recrystallization, grain refinement) in dendritic ensemble growing from the undercooled melts a detailed computational modeling should be carried out [44–46].

6 Conclusions

The developed sharp-interface model of dendritic solidification has been used to quantitatively estimate influence of tiny amounts of impurity and forced convection on the kinetics of dendritic growth. Using results of dendritic growth of a pure Ni and the Ni–Zr alloys a complicated behavior in predomination effects of convection and tiny amounts of impurity at different undercooling ranges is shown. This behavior, however, allows us to quantitatively estimate that (i) the tiny amount of impurity enhances the dendrite growth velocity in the lowest range of undercooling ($\Delta T < 10\,\mathrm{K}$ for diluted Ni–Zr alloy) and (ii) the forced incoming flow enhances the dendrite growth in the intermediate range of undercooling ($20 < \Delta T(\mathrm{K}) < 80$ for diluted Ni–Zr alloy). Thus, at least in the example of dendritic solidification of Ni and Ni–Zr alloys, the earlier idea that the solute effect shows a different temperature characteristics than the transport effect by fluid flow, which makes it possible to discriminate between both these effects by investigating the dendritic growth velocity as a function of undercooling is confirmed.

The authors acknowledge the support by the European Space Agency (ESA) under research project MULTIPHAS (AO-2004), the German Aerospace Center (DLR) Space Management under contract No. 50WM1541 and also from the Russian Science Foundation under the project no. 16-11-10095.

Author contribution statement

All authors contributed equally to the present research article.

References

1. D. Herlach, P. Galenko, D. Holland-Moritz, *Metastable solids from undercooled melts* (Elsevier, Amsterdam, 2007)

2. D.M. Herlach, D.M. Matson, *Solidification of containerless undercooled melts* (Weinheim, Wiley-VCH, 2012)
3. P.K. Galenko, O. Funke, J. Wang, D.M. Herlach, Mater. Sci. Eng. A **75377**, 488 (2004)
4. P.K. Galenko, D.M. Herlach, G. Phanikumar, O. Funke, Mater. Sci. Forum **508**, 431 (2006)
5. P.K. Galenko, D.M. Herlach, O. Funke, G. Phanikumar, in *Solidification and Crystallization* (2003), Vol. 52
6. D.M. Herlach, O. Funke, P. Gandham, P. Galenko, in *Solidification Processes and Microstructures: A Symposium in Honor of Wilfried Kurz* (2004), Vol. 277
7. D.M. Herlach, P.K. Galenko, Mater. Sci. Eng. A **449451**, 34 (2007)
8. D.V. Alexandrov, P.K. Galenko, D.M. Herlach, J. Cryst. Growth **312**, 2122 (2010)
9. D.V. Alexandrov, P.K. Galenko, J. Phys. A: Math. Theor. **46**, 195101 (2013)
10. D. Herlach, P. Galenko, J. Jpn. Soc. Microgravity Appl. **27**, 245 (2010)
11. D.V. Alexandrov, P.K. Galenko, Phys. Rev. E **87**, 062403 (2013)
12. D.V. Alexandrov, P.K. Galenko, Phys. Usp. **57**, 771 (2014)
13. D.V. Alexandrov, P.K. Galenko, Phys. Chem. **17**, 19149 (2015)
14. J. Gao, M. Han, A. Kao, K. Pericleous, D.V. Alexandrov, P.K. Galenko, Acta Mater. **103**, 184 (2016)
15. D.M. Herlach, S. Burggraf, P. Galenko, Ch.-A. Gandin, A. Garcia-Escorial, H. Henein, C. Karrasch, A. Mullis, M. Rettenmayr, J. Valloton, JOM **69**, 1303 (2017)
16. P.K. Galenko, K. Reuther, O.V. Kazak, D.V. Alexandrov, M. Rettenmayr, Appl. Phys. Lett. **111**, 031602 (2017)
17. P.K. Galenko, D.A. Danilov, K. Reuther, D.V. Alexandrov, M. Rettenmayr, D.M. Herlach, J. Crys. Growth **457**, 349 (2017)
18. O.V. Kazak, P.K. Galenko, D.V. Alexandrov, IOP Conf. Ser.: Mater. Sci. Eng. **192**, 012030 (2017)
19. J. Gao, A. Kao, K. Pericleous, P.K. Galenko, D.V. Alexandrov, J. Cryst. Growth **471**, 66 (2017)
20. D.V. Alexandrov, P.K. Galenko, L.V. Toropova, Philos. Trans. R. Soc. A **376**, 20170215 (2018)
21. A. Barbieri, J.S. Langer, Phys. Rev. A **39**, 5314 (1989)
22. M. Ben Amar, P. Pelcé, Phys. Rev. A **39**, 4263 (1989)
23. P.K. Galenko, D.A. Danilov, Phys. Lett. A **235**, 271 (1997)
24. P.K. Galenko, D.A. Danilov, J. Cryst. Growth **197**, 992 (1999)
25. D.V. Alexandrov, D.A. Danilov, P.K. Galenko, Int. J. Heat Mass Transfer **101**, 789 (2016)
26. M. Ben Amar, Physica D **31**, 409 (1988)
27. E. Brener, V.I. Melnikov, JETP **80**, 341 (1995)
28. J.S. Langer, D.C. Hong, Phys. Rev. A **34**, 1462 (1986)
29. P. Pelcé, D. Bensimon, Nucl. Phys. B **2**, 259 (1987)
30. P. Bouissou, P. Pelcé, Phys. Rev. A **40**, 6673 (1989)
31. H. Müller-Krumbhaar, T. Abel, E. Brener, M. Hartmann, N. Eissfeldt, D. Temkin, JSME Int. J. Ser. B **45**, 129 (2002)
32. E.A. Brener, J. Cryst. Growth **99**, 165 (1990)
33. W. Kurz, D.J. Fisher, Acta Metall. **29**, 11 (1981)
34. J. Lipton, M.E. Glicksman, W. Kurz, Mater. Sci. Eng. **65**, 357 (1984)
35. W.J. Boettinger, S.R. Coriell, Microstructure formation in rapidly solidified alloys, in *Science and Technology of the Undercooled Melt*, edited by P.R. Sahm, H. Jones, C.M. Adam (Springer, Netherlands, 1986)
36. J. Lipton, W. Kurz, R. Trivedi, Acta Metall. **35**, 957 (1987)
37. R. Trivedi, J. Lipton, W. Kurz, Acta Metall. **35**, 965 (1987)
38. W.J. Boettinger, S.R. Coriell, R. Trivedi, Application of dendritic growth theory to the interpretation of rapid solidification microstructures, in *Rapid Solidification Processing: Principles and Technologies IV*, edited by R. Mehrabian, P.A. Parrish (Claitor's, Baton Rouge, Louisiana, 1988)
39. P. Galenko, Phys. Rev. E **76**, 031606 (2007)

40. P. Galenko, Phys. Rev. B **65**, 144103 (2002)
41. H. Hartmann, P.K. Galenko, D. Holland-Moritz, M. Kolbe, D.M. Herlach, O. Shuleshova, J. Appl. Phys. **103**, 073509 (2008)
42. R.W. Hyers, Meas. Sci. Technol. **16**, 394 (2005)
43. P.K. Galenko, G. Phanikumar, O. Funke, L. Chernova, S. Reutzel, M. Kolbe, D.M. Herlach, Mater. Sci. Eng. A **449451**, 649 (2007)
44. V. Bojarevics, A. Kao, K. Pericleous, Modelling the fluid dynamics and dendritic solidification in EM-Levitated alloy melts, in *Solidification of Containerless Undercooled Melts*, edited by D.M. Herlach, D.M. Matson (Wiley-VCH Verlag, 2012)
45. T. Cool, P.W. Voorhees, Philos. Trans. R. Soc. A **376**, 20170213 (2018)
46. A. Kao, J. Gao, K. Pericleous, Philos. Trans. R. Soc. A **376**, 20170206 (2018)